LETTERS

Impacts of orbital forcing and atmospheric carbon dioxide on Miocene ice-sheet expansion

Ann Holbourn[1], Wolfgang Kuhnt[1], Michael Schulz[2] & Helmut Erlenkeuser[3]

The processes causing the middle Miocene global cooling, which marked the Earth's final transition into an 'icehouse' climate about 13.9 million years ago (Myr ago)[1–4], remain enigmatic. Tectonically driven circulation changes[5,6] and variations in atmospheric carbon dioxide levels[7,8] have been suggested as driving mechanisms, but the lack of adequately preserved sedimentary successions has made rigorous testing of these hypotheses difficult. Here we present high-resolution climate proxy records, covering the period from 14.7 to 12.7 million years ago, from two complete sediment cores from the northwest and southeast subtropical Pacific Ocean. Using new chronologies through the correlation to the latest orbital model[9], we find relatively constant, low summer insolation over Antarctica coincident with declining atmospheric carbon dioxide levels at the time of Antarctic ice-sheet expansion and global cooling, suggesting a causal link. We surmise that the thermal isolation of Antarctica played a role in providing sustained long-term climatic boundary conditions propitious for ice-sheet formation. Our data document that Antarctic glaciation was rapid, taking place within two obliquity cycles, and coincided with a striking transition from obliquity to eccentricity as the drivers of climatic change.

About 13.9 Myr ago, the Earth's climate cooled dramatically after an extended period of relative warmth. This key transition in the Earth's climatic and biotic evolution marked the final stage of stepwise Cenozoic cooling, and coincided with major ice-sheet expansion over Antarctica[1–4]. However, the timing, duration and driving mechanisms of this critical episode still remain largely unsolved, because sedimentary successions spanning this interval have been strongly affected by carbonate dissolution or burial diagenesis or proved incomplete owing to radical changes in ocean circulation. Thus, developing uninterrupted, high-resolution middle Miocene climate records that can be tied to an orbital timescale represents a major challenge for understanding the pacing and trigger of Cenozoic global cooling.

Here we present benthic foraminiferal oxygen ($\delta^{18}O$) and carbon ($\delta^{13}C$) isotope (4–5 kyr resolution) and X-ray fluorescence scanning (XRF) records (1-kyr resolution) in complete middle Miocene sedimentary sequences recovered at Ocean Drilling Program (ODP) Site 1146 (19° 27.40′ N, 116° 16.37′ E, 2,092 m) and Site 1237 (16° 0.421′ S, 76° 22.685′ W, 3,212 m) (Supplementary Information). These continuous successions allow unprecedented resolution of climate evolution on orbital timescales and permit detailed correlation of palaeoceanographic events in spatially separated regions in the northwest and southeast subtropical Pacific.

We developed orbitally tuned age models (Supplementary Information) by correlating the $\delta^{18}O$ records at each site to computed variations of the Earth's orbit and solar insolation (obliquity and eccentricity in ref. 9). The most salient features of the $\delta^{18}O$ time series are the major increase in values at 13.91–13.84 Myr ago (0.8‰ at Site 1237 and 1.2‰ at Site 1146), and the transition from high-amplitude obliquity-paced variations dominant between 14.7 and 13.9 Myr ago to eccentricity-paced fluctuations between 13.8 and 13.1 Myr ago (Figs 1 and 2). Higher-amplitude oscillations at Site 1146 (0.56‰ ± 0.12‰ versus 0.31‰ ± 0.15‰ mean amplitude at Site 1237) indicate a stronger temperature component in the 1146 $\delta^{18}O$ record between 14.7 and 13.9 Myr ago. Nevertheless, the global correlation of isotopic events and evidence for substantial Antarctic ice growth between 14.8 and 13.6 Myr ago[10] support that both $\delta^{18}O$ records closely track ice-volume fluctuations. Furthermore, benthic Mg/Ca temperature estimates indicate that most of the deep-sea $\delta^{18}O$ increase at 13.91–13.84 Myr ago can be attributed to an increase in continental ice volume[11]. The 100-kyr and 41-kyr signal components in $\delta^{18}O$ show amplitude modulation similar to that of the eccentricity and obliquity, with a striking transition from high amplitude in the 41-kyr band to high amplitude in the 100-kyr band at ~14.1–13.8 Myr ago (Fig. 2). The 100-kyr beat is also prominent in the 1237 Fe record after 14.1 Myr ago.

At first sight, the middle Miocene transition from a 41-kyr to 100-kyr world shows similarity to the 'Middle Pleistocene revolution' following an increase in Northern Hemisphere glaciation[12–14]. However, the middle Miocene transition differs in several aspects: (1) the middle Miocene 100-kyr cycles do not exhibit higher-amplitude variations than the 41-kyr cycles; (2) the transition from 41-kyr to 100-kyr periodicity occurred during or even before ice-sheet expansion without substantial time lag; (3) the middle Miocene 100-kyr cycles show a clear phase relationship and similar amplitude modulation to eccentricity, as well as both 125-kyr and 95-kyr components (Fig. 1, Supplementary Fig. S4). In contrast, the origin of the middle Pleistocene 100-kyr cycles remains puzzling, because their onset coincided with a period of weak eccentricity forcing[15].

Between 14.7 and 13.9 Myr ago, high amplitude in the 41-kyr band of the $\delta^{18}O$ signal (Fig. 2) suggests an already expanded Antarctic ice-sheet fluctuating in response to obliquity forcing. The ensuing $\delta^{18}O$ increase at 13.91–13.84 Myr ago, which marked the main increase in middle Miocene Antarctic glaciation, was also clearly modulated by obliquity (Figs 1 and 3). Obliquity controls the gradient in summer insolation between high and low latitudes, which drives the poleward atmospheric heat and moisture transfer[16]. Enhanced meridional moisture transport during periods of high differential heating between high and low latitudes at obliquity minima would promote ice-sheet growth, whereas a low summer insolation gradient at obliquity maxima would decrease poleward moisture transport, inhibiting ice-sheet build-up[16,17]. Similar obliquity-paced variations in moisture supply for the Holocene and late Pleistocene East Antarctic ice-sheet are evident from the deuterium excess record in the Vostok ice core[18]. High deuterium excess values during obliquity

[1]Institute of Geosciences, Christian-Albrechts-University, D-24118 Kiel, Germany. [2]Department of Geosciences and Research Center Ocean Margins, University of Bremen, Postfach 330 440, D-28334 Bremen, Germany. [3]Leibniz Laboratory for Radiometric Dating and Stable Isotope Research, Christian-Albrechts-University, D-24118 Kiel, Germany.

minima were related to an enhanced contribution of low latitude warm moisture sources leading to ice build-up, while during obliquity maxima cooler, local oceanic moisture sources dominated. In short, the prominent obliquity beat in benthic $\delta^{18}O$ before and during the major middle-Miocene ice-sheet expansion suggests that Southern Hemisphere ice growth was most probably primarily modulated by atmospheric heat and moisture transport, rather than by changing oceanic circulation patterns. On the other hand, ice-sheet dynamics may have in turn influenced oceanic circulation and heat transport. For instance, palaeocurrent reconstructions of the deep western boundary current reveal variability of the deep Pacific inflow on the 41-kyr timescale, with the highest current intensities during obliquity minima in the Pleistocene[19] and middle Miocene before 13.9 Myr ago[20].

Stepwise cooling of Antarctic Circumpolar surface waters before the expansion of the cryosphere was inferred from high-latitude Mg/Ca temperature records from the South Tasman Rise ODP Site 1171 (ref. 21). When the Site 1171 benthic $\delta^{18}O$ is correlated to the orbitally tuned records of Sites 1146 and 1237, sea surface temperature (SST) variations between 14.20 and 13.87 Myr ago appear strongly influenced by orbital forcing (Fig. 3). A remarkable feature of the Site 1171 records is that opposite trends between ice volume and SSTs occur between 14.20 and 13.87 Myr ago: cooling in Antarctic Circumpolar surface waters coincided overall with ice volume decreases (lower benthic $\delta^{18}O$) at increasing obliquity, whereas surface warming occurred during phases of ice build-up at decreasing obliquity (Fig. 3). These fluctuations are consistent with the notion that changing atmospheric heat and moisture supply drove ice volume on an obliquity timescale.

Between 14.05 and 13.87 Myr ago, three major cooling episodes occurred during an interval, when the amplitude of eccentricity increased (Fig. 3). This stepwise surface cooling was interpreted as eccentricity-paced intensification of the Antarctic Circumpolar Current, eventually leading to increased thermal isolation of Antarctica and global cooling[21]. However, it is intriguing that at least two of the three cooling episodes (centred at 14.04 and 13.88 Myr ago) coincided with decreasing benthic $\delta^{18}O$ (Fig. 3) and freshening of surface waters at Site 1171 (ref. 21). A fitting explanation may be that surface cooling was triggered by massive melting pulses, when the Antarctic ice sheet became unstable owing to the conjunction of increasing obliquity and high eccentricity favouring ice-sheet decay. The interval between 14.04 and 13.88 Myr ago was characterized by high-amplitude changes in insolation over Antarctica, and fluctuations in obliquity-driven heat and moisture supply would have led to ice-sheet instability and affected oceanic circulation. High-resolution deep-water temperature reconstructions to deconvolve ice volume and temperature in benthic $\delta^{18}O$ could potentially resolve the dynamics of Antarctic glaciation and its link to thermohaline circulation during this critical interval.

The main $\delta^{18}O$ increase after 13.9 Myr ago occurred during a

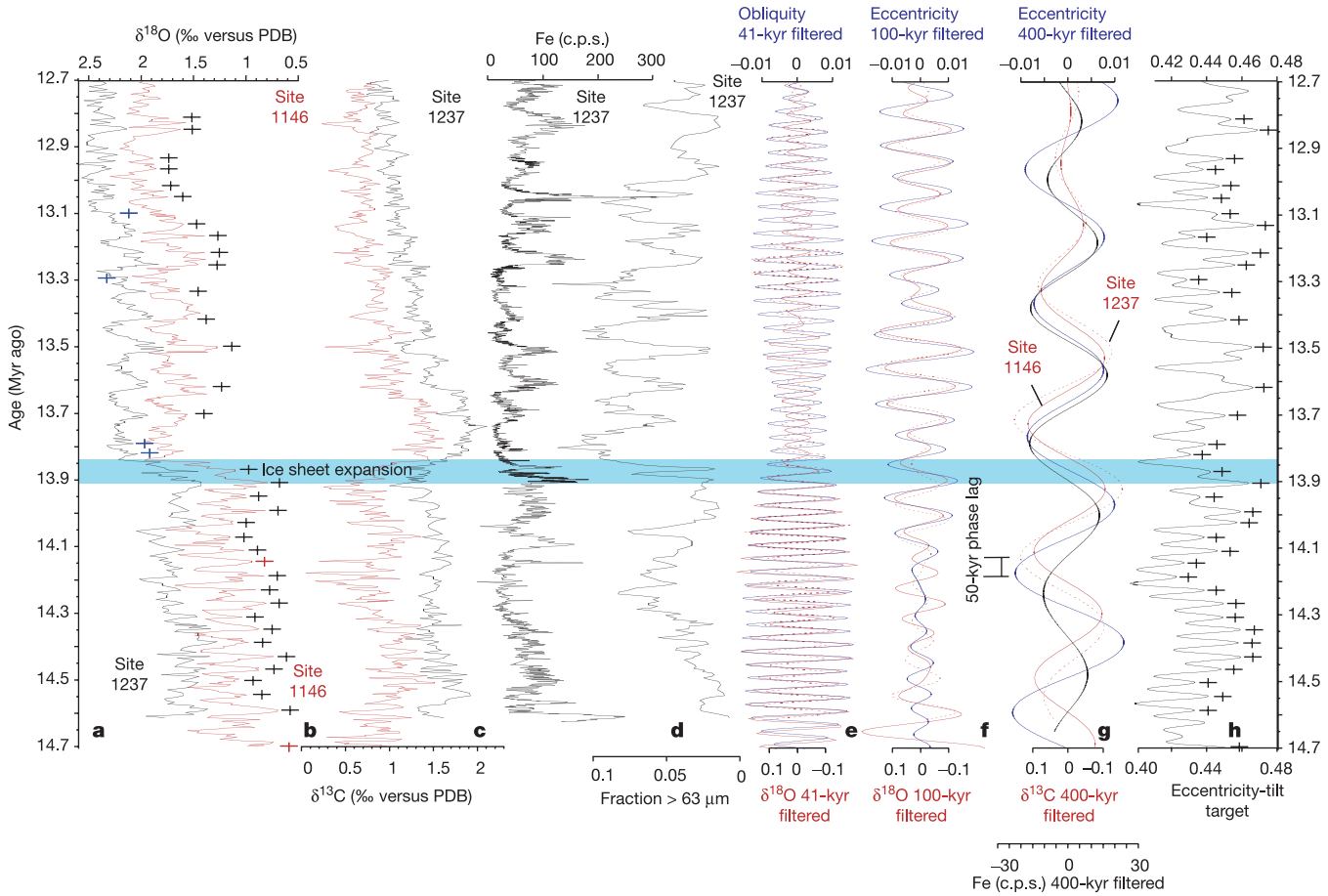

Figure 1 | Palaeoceanographic records from ODP Sites 1146 and 1237 showing that Earth's orbital configuration was the prime pacer of middle Miocene climate change. **a**, Benthic foraminiferal $\delta^{18}O$. Age control points marked by crosses (black, both sites; blue, Site 1237; red, Site 1146). **b**, Benthic foraminiferal $\delta^{13}C$. **c**, Site 1237 iron content in counts per second (c.p.s.). **d**, Site 1237 proportion of coarse fraction indicating increased carbonate preservation during colder periods corresponding to low eccentricity after 13.9 Myr ago. **e**, **f**, Comparison of filtered 41-kyr and 100-kyr $\delta^{18}O$, obliquity[9] and eccentricity[9] (Site 1146, solid red line; Site 1237, dotted red line). **g**, Comparison of 400-kyr-filtered iron contents, $\delta^{13}C$ and eccentricity[9]. **h**, Eccentricity-tilt tuning target. Age correlation points marked by crosses.

period when eccentricity declined and amplitude variations in obliquity decreased (Fig. 3). This orbital configuration would have resulted in an extended period of low seasonal contrast over Antarctica, inhibiting summer melting and favouring ice-sheet expansion. Such an orbital configuration is not unique, and recurs approximately every 2.4 million years without inevitably inducing major ice growth. A further factor influencing Antarctic glaciation after 13.9 Myr ago may have been a coeval decrease in atmospheric CO_2 partial pressure (p_{CO_2}). Marine $\delta^{13}C$ is closely linked to p_{CO_2} through productivity and organic carbon burial feedbacks resulting in the lowest p_{CO_2} at $\delta^{13}C$ maxima and the highest p_{CO_2} at $\delta^{13}C$ minima[22]. A prominent feature of the middle Miocene $\delta^{13}C$ curve is the positive excursion starting at 13.92 Myr ago with the maximum centred at ~13.7 Myr ago, which represents the final and most pronounced $\delta^{13}C$ increase and p_{CO_2} decrease within the 'Monterey Excursion'[8].

Enhanced carbonate preservation after 13.9 Myr ago could have contributed to increased organic carbon burial, because the rate of burial also depends on the residence time of carbon in the mixed sediment surface layer, and hence carbonate accumulation rates[23,24]. Increased carbonate preservation, evident at the deeper Site 1237 after 13.9 Myr ago (Fig. 1), may be representative for large areas of the subtropical Pacific. It was probably related to a reduction of the shelf carbonate reservoir due to falling sea level and improved deep-water ventilation, and bears similarity to the rapid deepening of the Calcite Compensation Depth (CCD) near the Eocene–Oligocene boundary when permanent ice sheets appeared on Antarctica[25]. Indeed, the 1237 Fe and the $\delta^{13}C$ records at Sites 1146 and 1237 are significantly coherent ($\alpha = 0.1$, not shown) with the 400-kyr eccentricity cycle between 14.3 and 13.1 Myr ago (Fig. 1). Whereas Fe (carbonate dissolution) is in phase with the 400-kyr eccentricity cycle, $\delta^{13}C$ exhibits a ~50 kyr phase lag (Fig. 1), indicating that the Pacific carbon cycle influenced $\delta^{13}C$. The $\delta^{13}C$ minimum at 13.92 Myr ago occurs before the onset of the major $\delta^{18}O$ increase at 13.91 Myr ago. Interestingly, a minimum in the 400-kyr $\delta^{13}C$ cycle also precedes the $\delta^{18}O$ increase at the Oligocene–Miocene boundary[26]. Thus, the 400-kyr eccentricity cycle appears strongly to influence the carbon cycle[27], and may even modulate long-term climate evolution.

Our results indicate that a conjunction of climatic forcing factors ultimately triggered middle-Miocene ice-sheet expansion and global cooling. Between 14.7 and 13.84 Myr ago, ice volume was strongly modulated by obliquity-paced atmospheric moisture transfer. A change in eccentricity cadence (from 400 to 100 kyr) led initially to ice-sheet decay and instability from 14.05 to 13.87 Myr ago. However, the ice-sheet expanded rapidly at 13.87–13.84 Myr ago during an extended interval of low seasonal contrast at low eccentricity that coincided with a prominent $\delta^{13}C$ increase. We surmise that changing boundary conditions, in particular decreasing p_{CO_2}, primed the dramatic response of the climate system that marked the final step into the 'icehouse' climate. Atmospheric CO_2 fluctuations influencing climate evolution on orbital timescales have not been resolved by previous work[28,29], and higher-resolution p_{CO_2} proxy records are urgently needed to clarify the role of atmospheric CO_2 in Cenozoic climate cooling.

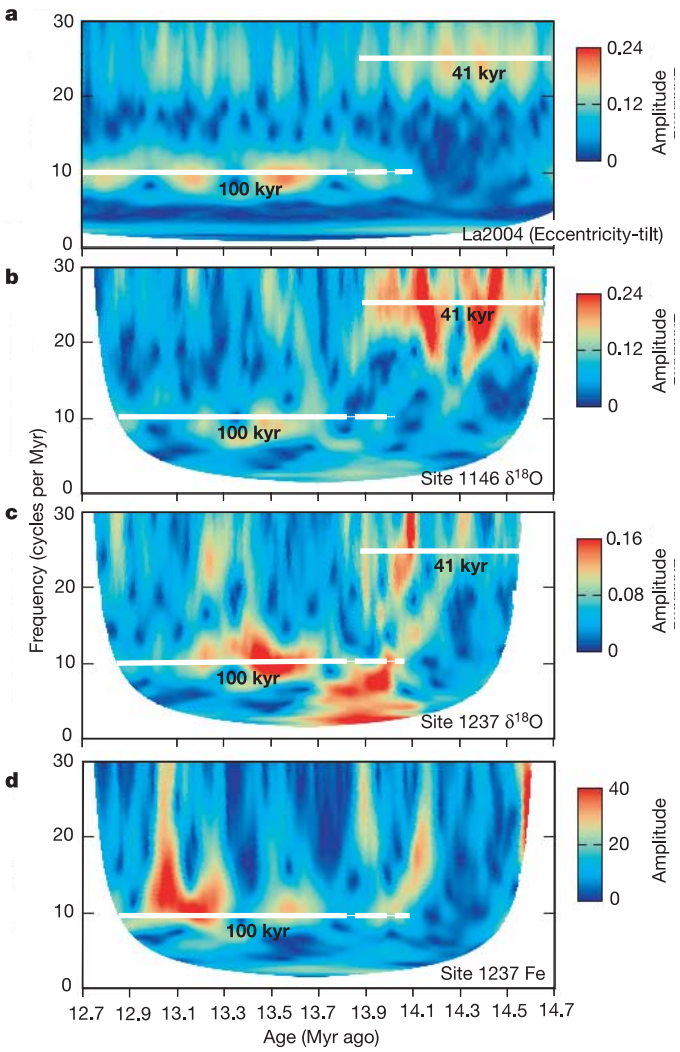

Figure 2 | Signal evolution in time–frequency space of $\delta^{18}O$ and Fe in ODP Sites 1146 and 1237 and of eccentricity-tilt tuning target. The amplitude evolution in the 100-kyr and 41-kyr bands of $\delta^{18}O$ follows eccentricity and obliquity. Deep-water cooling and Antarctic ice-sheet expansion coincided with a transition from 41-kyr to 100-kyr periodicity in $\delta^{18}O$. Signal amplitudes are in same units as data analysed. La2004 refers to the orbital solution in ref. 9 (Laskar *et al.*, 2004).

METHODS

Chronology. New chronologies were generated by initially matching the 400-kyr and 100-kyr amplitude variations in the $\delta^{18}O$ series to the latest astronomical solution[9], and then fine-adjusting individual obliquity-scale cycles. As tuning target, we constructed an eccentricity-tilt composite with no phase shift and equal weight of eccentricity and obliquity (Supplementary Information). Age tiepoints are given in Fig. 1 and Supplementary Tables S3 and S4. We tuned $\delta^{18}O$ minima to obliquity maxima, since we assumed (1) that relatively warm summers during high obliquity would promote ice-sheet melting in Antarctica, whereas cool summers during low obliquity would favour ice-sheet growth, and (2) that a low summer insolation gradient between low and high latitudes during high obliquity would decrease poleward moisture transport, inhibiting ice-sheet build-up[17]. We did not adjust our tuning for possible phase lags between $\delta^{18}O$ and insolation forcing, since the response time of a smaller middle Miocene Antarctic ice-sheet is unknown. We applied gaussian band-pass filters to the 1146 and 1237 $\delta^{18}O$ and 1237 Fe series to extract oscillations associated with the 400, 100 and 41 kyr periods. Gaussian band-pass filters were centred at 0.0244 kyr^{-1} (41-kyr period) with 0.005 kyr^{-1} bandwidth (34.0–51.5-kyr period), 0.01 kyr^{-1} (100-kyr period) with 0.003 kyr^{-1} bandwidth (76.9–142.9-kyr period) and 0.0025 kyr^{-1} (400-kyr period) with 0.0005 kyr^{-1} bandwidth (333.3–500.0-kyr period). $\delta^{18}O$ is phase-locked with obliquity in the 41-kyr band, and the amplitude modulation of the 41-kyr filtered signals closely follows obliquity between 14.7 and 13.5 Myr ago (Fig. 1). The amplitude of the 100-kyr filtered $\delta^{18}O$ and Fe signals increases after 14.1 Myr ago, exhibiting similar modulation as eccentricity (Figs 1 and 2). Spectral analysis of the $\delta^{18}O$, Fe and coarse residue time series reveal strong power at all Milankovitch frequency bands, except precession (Supplementary Fig. S4). The spectral peak for short eccentricity shows a characteristic split into 95-kyr and 125-kyr periods. Spectral power in the short and long eccentricity periods are enhanced after tuning to obliquity.

Time–frequency analysis. Temporal changes in amplitude of signal components were estimated over a predefined range of frequencies using a harmonic-filtering algorithm[30], which fits sinusoidal waves to a time series by means of least-squares. This method can process unevenly spaced time series directly. To obtain

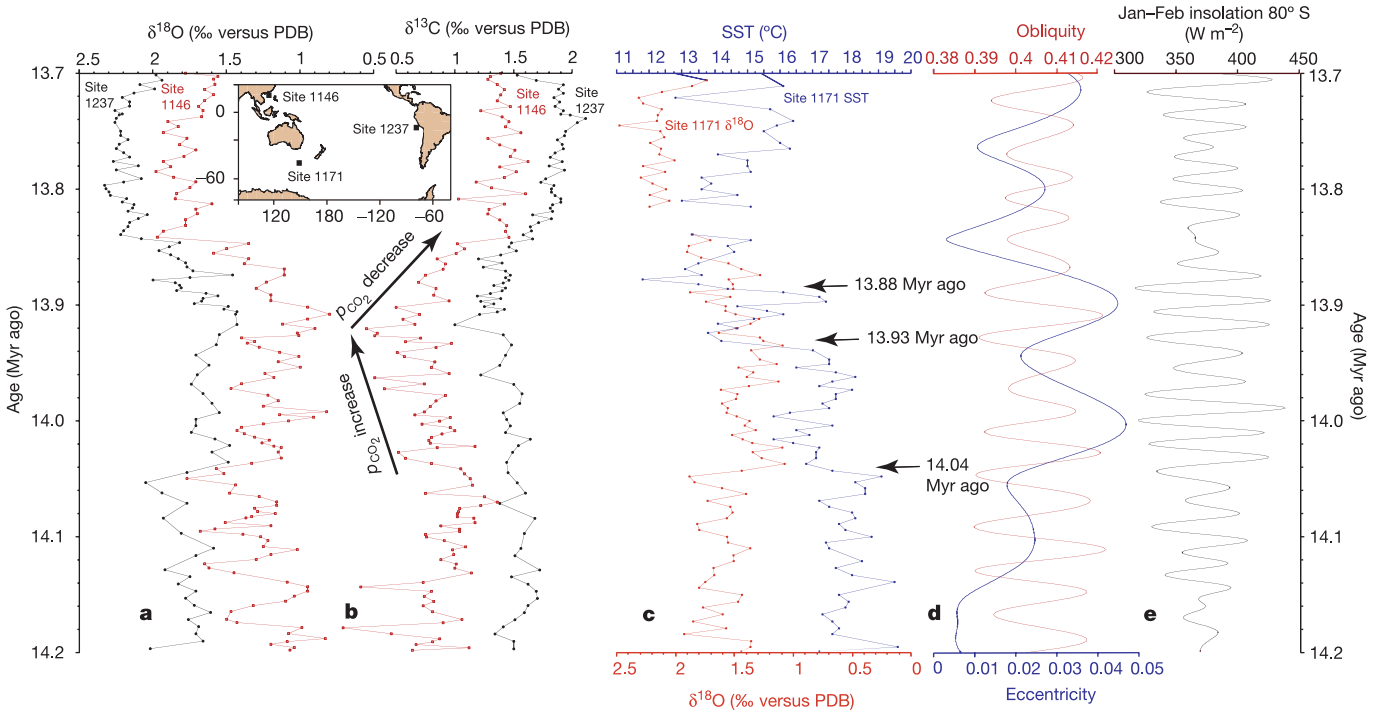

Figure 3 | Expanded view of 14.2–13.7 Myr ago interval. a, b, Climate proxies are same as in Fig. 1. A minimum in $\delta^{13}C$ reflecting a maximum in atmospheric p_{CO_2} preceded ice-sheet expansion and global cooling. This $\delta^{13}C$ minimum, indicated by arrows in **b**, marks the turning point of the 400-kyr cycle at 13.92 Myr ago. **c**, Benthic $\delta^{18}O$ and SSTs at South Tasman Rise ODP Site 1171 (ref. 21). Arrows indicate prominent, rapid surface cooling events preceding cryosphere expansion. **d**, Obliquity and eccentricity[9]. **e**, January–February insolation at 80° S (ref. 9). The conjunction of low eccentricity and low obliquity resulted in an extended period of low seasonality over Antarctica between 13.87–13.83 Myr ago.

time-dependent amplitude estimates, the input time series is analysed within a moving window of width $T_w = w \times T_f$, where $w = 3$ is a width factor and T_f denotes the signal periodicity of interest (for example, 400 kyr). The resulting amplitude of the best-fit sinusoid is plotted versus the average of the observation times within the current segment. The dependence of window width T_w on frequency leads to a change in temporal resolution with frequency, similar to wavelet analysis (see Supplementary Information for further details).

Isotope analysis. We measured $\delta^{18}O$ and $\delta^{13}C$ in epifaunal benthic foraminifers (*Planulina wuellerstorfi* or *Cibicidoides mundulus* except in ten samples from Site 1146, where we analysed *C. barnetti* or *C. incrassatus*). Well-preserved tests were broken into large fragments, cleaned in alcohol in an ultrasonic bath, then dried at 40 °C. Measurements were made with the Finnigan MAT 251 mass spectrometer at the Leibniz Laboratory, Kiel University. The instrument is coupled on-line to a Carbo-Kiel Device (Type I). Samples were reacted by individual acid addition (99% H_3PO_4 at 73 °C). The standard external error is better than ±0.07‰ and ±0.05‰ for $\delta^{18}O$ and $\delta^{13}C$, respectively. Replicate measurements on ~7% of samples indicate mean reproducibility better than ±0.11‰ and ±0.13‰ for $\delta^{18}O$ and $\delta^{13}C$, respectively. Paired measurements in 37 samples indicate no significant offset in $\delta^{18}O$ and $\delta^{13}C$ between *P. wuellerstorfi* and *C. mundulus*. Results were calibrated using the National Institute of Standards and Technology (Gaithersburg, Maryland) carbonate isotope standard NBS 20 and NBS 19 and 18, and are reported on the PeeDee belemnite (PDB) scale.

XRF scanning. We performed XRF measurements with 1-cm resolution on the archive halves of the Site 1237 splice using the XRF Core Scanner at the Bremen ODP Core Repository. Overlapping measurements (50–100 cm) were made at correlation points to verify the accuracy and completeness of the splice. We interpreted Fe maxima as intervals of increased carbonate dissolution caused by poor deep-water ventilation and not as intervals of increased terrigenous dust flux or river run-off, based on the covariance of Fe and Mg, and the lack of covariance of Fe and Ti (Supplementary Fig. S5).

Received 21 February; accepted 4 August 2005.

1. Flower, B. P. & Kennett, J. P. Middle Miocene ocean-climate transition: high resolution oxygen and carbon isotopic records from DSDP Site 588A, southwest Pacific. *Paleoceanography* **8,** 811–843 (1993).
2. Flower, B. P. & Kennett, J. P. Middle Miocene deep water paleoceanography in the southwest Pacific: Relations with East Antarctic ice sheet development. *Paleoceanography* **10,** 1095–1112 (1995).
3. Miller, K. G., Wright, J. D. & Fairbanks, R. G. Unlocking the ice house: Oligocene-Miocene oxygen isotopes, eustacy and margin erosion. *J. Geophys. Res.* **96,** 6829–6848 (1991).
4. Zachos, J., Pagani, M., Sloan, L., Thomas, E. & Billups, K. Trends, rhythms, and aberrations in global climate 65 Ma to present. *Science* **292,** 686–693 (2001).
5. Kennett, J. P. Cenozoic evolution of Antarctic glaciation, the Circum-Antarctic Ocean and their impact on global paleoceanography. *J. Geophys. Res.* **82,** 3843–3860 (1975).
6. Woodruff, F. & Savin, S. Mid-Miocene isotope stratigraphy in the deep sea: high resolution correlations, paleoclimatic cycles, and sediment preservation. *Paleoceanography* **6,** 755–806 (1991).
7. Raymo, M. E. & Ruddiman, W. F. Tectonic forcing of late Cenozoic climate. *Nature* **359,** 117–122 (1992).
8. Vincent, E. & Berger, W. H. in *The Carbon Cycle and Atmospheric CO_2: Natural Variations Archean to Present* (eds Broecker, W. S. & Sundquist, E. T.) 455–468 (Geophys. Monogr. Ser. 32, AGU, Washington DC, 1985).
9. Laskar, J. *et al.* A long term numerical solution for the insolation quantities of the Earth. *Astron. Astrophys.* **428,** 261–285 (2004).
10. Sugden, D. & Denton, G. Cenozoic landscape evolution of the Convoy Range to Mackay Glacier area, Transantarctic Mountains: Onshore to offshore synthesis. *Geol. Soc. Am. Bull.* **116,** 840–857 (2004).
11. Lear, C. H., Elderfield, H. & Wilson, P. A. Cenozoic deep-sea temperature and global ice volumes from Mg/Ca in benthic foraminiferal calcite. *Science* **287,** 269–272 (2000).
12. Berger, W. H. & Jansen, E. in *The Polar Oceans and their Role in Shaping the Global Environment* (eds Johannessen, O. M., Muench, R. D. & Overland, J. E.) 295–311 (Geophys. Monogr. Ser. 85, AGU, Washington, DC, 1994).
13. Mudelsee, M. & Schulz, M. The Middle Pleistocene climate transition: onset of 100 kyr cycle lags ice volume buildup by 280 ka. *Earth Planet. Sci. Lett.* **151,** 117–123 (1997).
14. Shackleton, N. J. The 100,000-year ice-age cycle identified and found to lag temperature, carbon dioxide, and orbital eccentricity. *Science* **289,** 1897–1902 (2000).
15. Imbrie, J. *et al.* On the structure and origin of major glaciation cycles. 2. The 100,000 years cycle. *Paleoceanography* **8,** 699–735 (1993).
16. Raymo, M. E. & Nisancioglu, K. The 41 kyr world: Milankovitch's other unsolved mystery. *Paleoceanography* **18,** 1011 doi:10.1029/2002PA00791 (2003).
17. Loutre, M.-F., Paillard, D., Vimeux, F. & Cortijo, E. Does mean annual insolation have the potential to change the climate? *Earth Planet. Sci. Lett.* **221,** 1–14 (2004).

18. Vimeux, F. *et al.* A 420,000 year deuterium excess record from East Antarctica: Information on past changes in the origin of precipitation at Vostok. *J. Geophys. Res.* **106,** 31863–31873 (2001).
19. Hall, I. R., McCave, N., Shackleton, N. J., Weedon, G. P. & Harris, S. Intensified deep Pacific inflow and ventilation in Pleistocene glacial times. *Nature* **412,** 809–812 (2001).
20. Hall, I. R. *et al.* Paleocurrent reconstruction of the deep Pacific inflow during the middle Miocene: Reflections of Antarctic Ice Sheet growth. *Paleoceanography* **18,** 1040–1051 (2003).
21. Shevenell, A. E., Kennett, J. P. & Lea, D. W. Middle Miocene Southern Ocean cooling and Antarctic cryosphere expansion. *Science* **305,** 1766–1770 (2004).
22. Kump, L. R. & Arthur, M. A. Interpreting carbon-isotope excursions: carbonate and organic matter. *Chem. Geol.* **161,** 181–198 (1999).
23. Müller, P. J. & Suess, E. Productivity, sedimentation rate, and sedimentary organic matter in the oceans. 1. Organic carbon preservation. *Deep-Sea Res. A* **26,** 1347–1362 (1979).
24. Jahnke, R. A. The global ocean flux of particulate organic carbon: Areal distribution and magnitude. *Glob. Biogeochem. Cycles* **10,** 71–88 (1996).
25. Coxhall, H. K., Wilson, P. A., Pälike, H., Lear, C. H. & Backman, J. Rapid stepwise onset of Antarctic glaciation and deeper calcite compensation in the Pacific Ocean. *Nature* **433,** 53–57 (2005).
26. Zachos, J., Shackleton, N. J., Revenaugh, J. S., Pälike, H. & Flower, B. P. Climate response to orbital forcing across the Oligocene-Miocene boundary. *Science* **292,** 274–278 (2001).
27. Wang, P., Tian, J., Cheng, X., Liu, C. & Xu, J. Carbon reservoir changes preceded major ice-sheet expansion at the mid-Brunhes event. *Geology* **31,** 239–242 (2003).
28. Pagani, M., Arthur, M. A. & Freeman, K. H. Miocene evolution of atmospheric carbon dioxide. *Paleoceanography* **14,** 273–292 (1999).
29. Pearson, P. N. & Palmer, M. R. Atmospheric carbon dioxide concentrations over the past 60 million years. *Nature* **406,** 695–699 (2000).
30. Ferraz- Mello, S. Estimation of periods from unequally spaced observations. *Astron. J.* **86,** 619–624 (1981).

Supplementary Information is linked to the online version of the paper at www.nature.com/nature.

Acknowledgements We thank the Shipboard Scientific Parties of the Ocean Drilling Program (ODP) Legs 184 and 202, J. Kennett, U. Röhl, M. Sarnthein, A. Shevenell, J. Schönfeld, J. Stoner and J. Zachos for discussions. This research used samples provided by the ODP, and was funded by the Deutsche Forschungsgemeinschaft.

Author Information Data sets are archived at WDC-MARE (http://www.pangaea.de). Reprints and permissions information is available at npg.nature.com/reprintsandpermissions. The authors declare no competing financial interests. Correspondence and requests for materials should be addressed to A.E.H. (ah@gpi.uni-kiel.de).